The International Journal of Advanced Manufacturing Technology (2019) 101:1903–1913
https://doi.org/10.1007/s00170-018-3055-x

ORIGINAL ARTICLE

# Multi-objective optimization of mechanical quality and stability during micro resistance spot welding

Feng Chen[1] · Yusheng Wang[2] · Shiding Sun[3] · Zhenwu Ma[4] · Xiang Huang[1]

Received: 15 January 2018 / Accepted: 18 November 2018 / Published online: 26 November 2018


**Abstract**
Advancement of micro-joining methods has become an essential prerequisite in the manufacture of micro devices at ever smaller scales. For complex environments, micro joints must possess comprehensive mechanical quality and stability. Micro resistance spot welding has thus been identified as a promising technology in industrial applications. In this study, multi-objective optimization during welding of ultra-thin Ti-1Al-1Mn foils was investigated. The experiments, based on the Taguchi L27 orthogonal array, examined the effects and interactions of process parameters (ramp time, welding time, welding current, and electrode force) on important characteristics (tensile-shear force, weld nugget size and failure energy, and their variances). The hybrid optimization approach, comprising principal component analysis and gray relational analysis, was used for data processing, whereupon a back-propagation artificial neural network was used to establish a predictive model, taking advantage of a genetic algorithm to find the optimal parameters. The optimal set of welding parameters was found to be a ramp time of 2.7 ms, a welding time of 6.8 ms, a welding current of 800 A, and an electrode force of 31.6 N. Experiments validated the feasibility of the hybrid optimization approach, and an improvement of each response was found under the optimal welding conditions.

**Keywords** Titanium alloy · Micro welding · Mechanical properties · Optimization

## 1 Introduction

The demand on micro devices has increased extensively because of the ongoing trend in product miniaturization and multifunction [1–4]. Advancement of micro-joining methods has therefore become an essential prerequisite for manufacturing these devices. Among the numerous micro-joining technologies, micro resistance spot welding (MRSW) is a simple and applicable method applied in many fields because of its low hardware and processing costs [5–8]. MRSW belongs to a class of resistance welding that produces metallurgical bonding between surfaces by resistance heating. Thus, the quality of the joints depends on the heating processes, including generation, transmission, and dissipation, which are determined in turn by the welding parameters.

To obtain structurally sound, detect-free, and low-cost welds, the design of the welding parameters is usually characterized by the base material thickness [9]:

$$I = 3937 \times (t_1 + t_2)\ \mathrm{A} \tag{1}$$

$$F = 876 \times (t_1 + t_2)\ \mathrm{N} \tag{2}$$

$$T = 2.36 \times (t_1 + t_2)\ \text{cycles} \tag{3}$$

where $t_1$ and $t_2$ are the thicknesses of the upper and lower base materials, respectively, $I$ is the welding current, $F$ is the electrode force, and $T$ is the welding time.

Compared with normal-scale resistance spot welding (NSRSW), MRSW refers to the welding of ultra-thin materials (less than 0.2 mm thick) and has different welding parameters to those of NSRSW. For example, a smaller electrode and a much lower electrode force are usually adopted in MRSW.

✉ Feng Chen
fchen0526@nuaa.edu.cn

[1] College of Mechanical and Electrical Engineering, Nanjing University of Aeronautics and Astronautics, 29 Yudao St, Nanjing 210016, China

[2] AVIC Cheng Du Aircraft Industrial (Group) Co., Ltd, Chengdu, China

[3] Electrical and Computer Engineering, University of Nebraska-Lincoln, Lincoln, NE, USA

[4] College of Mechanical Engineering, Suzhou University of Science and Technology, Suzhou, China

These confine the area for current flow, thus creating a high-density energy source, a greater heating rate, and a higher peak temperature. Internal water cooling is not used for these small-scale electrodes, which can increase the possibility of electrode sticking. In addition, during the MRSW process, the welding current is concentrated in a region under the electrode. Thus, a traditional heat-affected zone is not observed [10], but excessive resistance heat may induce grain coarsening around the weld nugget in the base material. Therefore, the conventional welding parameters listed in Eqs. (1)–(3) are no longer applicable for the MRSW process. Instead, it is necessary to conduct parameter optimization for structurally sound, defect-free, and satisfactory performance welds during MRSW. Furthermore, to meet the requirements for micro devices, mechanical quality should be taken into consideration.

Various optimization and parameter-selection methods for resistance welding have been used for practical applications. Studies that (i) established the relationship between process parameters and welding quality, (ii) optimized the welding parameters, or (iii) predicted the welding quality have been widely reported [11–27]. Other investigations [28–34] have focused on on-line quality-monitoring systems for resistance spot welding, where selected features are extracted from the measured electrical signal. The effect of the welding parameters on the extracted features and the correlation between these features and the welding quality have both been analyzed. Typical studies are listed in Tables 1 and 2.

However, little work has been reported on micro-welding of ultra-thin metal foils, even though the application of these materials is ever-increasing. Validation of characteristic optimization in MRSW remains to be studied, taking in to account the size effect due to the sharp decrease in base material thickness. Furthermore, resistance spot welding shows a large variation in weld quality, which requires more welds to be performed than would be needed if each one was made reliably. However, the variation of mechanical quality in MRSW is much less than that in NSRSW [18]. The acceptable quality variation is related to target size, and less variation should be obtained when the target size decreases. Thus, both the mechanical quality and the consistency should be considered in order to obtain excellent composite weld quality in MRSW.

In our previous study [35], we investigated the effect of welding parameters on the tensile shear force, the peel force, and their variances. A hybrid approach, namely Taguchi-based gray relational analysis (GRA) coupled with principal component analysis (PCA), was shown to perform local optimization effectively. However, that approach could find the optimal welding conditions for only a fixed combination of welding parameters and was not applicable to global optimization. Moreover, in our previous study, several other important welding performance characteristics were not investigated. Therefore, an improved method is proposed herein to allow further research on MRSW to be conducted.

In the present study, to improve the multiple mechanical quality characteristics including larger values of tensile shear force, weld nugget size and failure energy, and smaller values of their variations, welding parameter optimization during MRSW of ultra-thin Ti-1Al-1Mn foils was performed based on the Taguchi method. Multiple mechanical qualities were converted into a comprehensive performance index by means of GRA coupled with PCA. After the prediction model was established, the optimum welding parameter values were specified using an artificial neural network (ANN)-based genetic algorithm (GA) optimization method.

**Table 1** Studies related to optimization in resistance spot welding

| Reference | Materials | Welding parameters | Optimization objectives | Optimization methods |
|---|---|---|---|---|
| Kim 2005 | steel | $I_w$, $T_w$, $F$ | $f_{ts}$, $h_i$ | RSM |
| Esme 2009 | steel | $I_w$, $T_w$, $F$, $D$ | $f_{ts}$, $h_i$ | TM |
| Luo 2009 | steel | $I_p$, $I_w$, $T_w$, $F$ | $d_n$, $\eta$, $f_{ts}$, | RA |
| Boriwal 2011 | steel δ:0.8 mm | $I_w$, $T_w$, $F$ | $d_n$, $f_{ts}$, $f_p$ | RA |
| Muhammad 2012 | steel δ:1 mm,1.5 mm | $I_w$, $T_w$, $T_h$ | $d_n$, $d_{HAZ}$ | TM, RSM |
| Pashazadeh 2014 | Steel δ:0.7 mm | $I_w$, $T_w$, $F$ | $d_n$, $h_N$ | ANNS, GA |
| Zhao 2013 | Ti-alloy δ:0.4 mm | $I_w$, $T_w$, $F$ | $d_n$, $\eta$, $f_{ts}$, $e$ | PCA, RSM |
| Zhao 2014 | Ti-alloy δ:0.4 mm | $I_w$, $T_w$, $F$ | $E$ | TM, RSM |
| Wan 2016 | Ti-alloy δ:0.4 mm | $I_w$, $T_w$, $F$ | $d_n$, $f_{ts}$, $l_{ts}$, $e$ | PCA, GA |
| Wan 2016 | Ti-alloy δ:0.4 mm | $I_w$, $T_w$, $F$ | $d_n$, $f_{ts}$, $l_{ts}$, $e$ | GRA, ANNS, GA |
| Wan 2016 | Ti-alloy δ:0.4 mm | $I_w$, $T_w$, $F$ | $d_n$, $f_{ts}$, $e$ | GRA, RA, GA, DF, ANNS, PCA |

$\delta$ thickness of base material, $T_w$ welding time, $I_w$ welding current, $I_p$ preheating current, $F$ electrode force, $T_h$ holding time, $T_s$ squeeze time, $D$ electrode diameter, $d_n$ nugget diameter, $h_n$ nugget height, $h_i$ indentation thickness, $\eta$ penetration rate, $d_{HAZ}$ heat-affected zone size, $f_{ts}$ tensile-shear failure load, $f_p$ peel force, $l_{ts}$ failure displacement, $e$ failure energy, $m$ failure mode, *GRA* gray relational analysis, *ANNS* artificial neural networks, *GA* genetic algorithm, *TM* Taguchi method, *RSM* response surface methodology, *RA* regression analysis, *PCA* principal component analysis, *DF* desirability function

**Table 2** Studies related to weld quality prediction in resistance spot welding

| Reference | Materials | Welding parameters | Monitoring index | Prediction objectives | Prediction methods |
|---|---|---|---|---|---|
| El-Banna 2008 | Steel δ:2 mm,0.85 mm | $T_w$ | DR | $d_n$, $m$ | ANNS |
| Zhang 2015 | Steel-1 δ:0.7 mm | $T_w$, $I_w$ | ED | $f_{ts}$ | |
| Chen 2016 | Ti-alloy δ:1.8 mm | | EC, EV, ED, EP | | |
| Adams 2017 | Steel-4 δ:0.6 mm | | DR | $f_{ts}$ | PCA |
| Wan 2017 | Ti-alloy δ:0.4 mm | $T_w$, $I_w$, $F$ | DR, EV | $f_{ts}$ | ANNS |
| Xing 2018 | Steel δ:1 mm | $T_w$, $I_w$, $F$ | DR | $f_{ts}$ | RF |

$\delta$ thickness of base material, $T_w$ welding time, $I_w$ welding current, $I_p$ preheating current, $F$ electrode force, $T_h$ holding time, $T_s$ squeeze time, $d_n$ nugget diameter, $h_n$ nugget height, $\eta$ penetration rate, $d_{HAZ}$ heat-affected zone size, $f_{ts}$ tensile-shear failure load, $f_p$ peel force, $l_{ts}$ failure displacement, $e$ failure energy, $m$ failure mode, *GRA* gray relational analysis, *ANNS* artificial neural networks, *GA* genetic algorithm, *TM* Taguchi method, *RSM* response surface methodology, *RA* regression analysis, *PCA* principal component analysis, *DF* desirability function, *RF* random forest, *DR* dynamic resistance, *EV* electrode voltage, *ED* electrode displacement, *EP* electrode pressure, *EC* electrode current

## 2 Experimental procedure

Ti-1Al-1Mn ultra-thin foils (0.05 mm in thickness) were selected as the base material for MRSW. The chemical composition was Al (1.8 wt%), Mn (1.8 wt%), Fe (0.05 wt%), C (0.01 wt%), N (0.02 wt%), O (0.13 wt%), H (0.002 wt%), and Ti (balance), with a yield strength of 622 MPa and an ultimate tensile strength of 683.5 MPa.

The input parameters were set as the ramp time ($T_r$), welding time ($T_w$), welding current ($I$), and electrode force ($F$), and the other welding parameters were fixed for all series, as specified in Table 3. To investigate the effect of each welding parameter and their combinations on mechanical quality and stability, the electrode was replaced every time, after the new welding parameters were established.

Tensile-shear tests were conducted at a tension rate of 0.2 mm/min at room temperature. An example specimen is shown in Fig. 1. The spot weld was performed in the center of two ultra-thin foils, and then, the specimen was cut using wire cutting based on the ASTM-E345 standard [36]. The weld nugget size was determined using a failed specimen after tensile-shear tests with a microscope. Each experiment was repeated five times, and the mean values were calculated for the tensile-shear force, nugget size, and failure energy. Their variations were calculated using Eq. (4).

$$S = \left(\frac{1}{5}\sum_1^5 (x_i - \bar{x})\right)^{1/2}, \bar{x} = \frac{1}{5}\sum_i^5 x_i \quad (4)$$

where $x_i$ is the experimental value, and each experiment was repeated five times.

**Table 3** Micro resistance spot welding conditions

| | Welding conditions |
|---|---|
| Model number | Hanson 4000 |
| Weld head | Hanson Ap-2 |
| Polarity | Medium frequency |
| Mode of operation | Constant current mode |
| Cooling mode | Air cooling |
| Shielding gas | No |
| Electrode | Cu-Cr-Zr |
| Electrode diameter | 5 mm |
| Squeeze time | 5 ms |
| Holding time | 1000 ms |

## 3 Multi-objective optimization design

Some important welding parameters for mechanical quality and stability were considered simultaneously, namely, tensile-shear force, weld nugget size, failure energy, and their respective variations. The tensile-shear force (f), weld nugget size (d), and failure energy (e) were classed as being the higher the better (HB), whereas their variations (fv, dv, and ev, respectively) were classed as being the lower the better (LB). Generally, improvement in one response may be detrimental to another response [37]. Therefore, GRA was applied to convert the six responses into one composite quality index (CQI), and final welding-parameter optimization was based on maximizing CQI. In other studies, the contribution of each response was either made equal or was determined by experience in GRA. However, that approach is not always applicable [38], especially for considering the quality and stability of welded joints after MRSW because of the complexity and lack of systemic research in this field. In the present work, PCA was conducted to determine the weighted factors for each response based on the experimental values. After calculating the CQI, a prediction model for it and the welding parameters was established by means of a back-propagation artificial neural network (BP-ANN). Finally, optimal welding parameters for maximizing the CQI were specified through a GA approach.

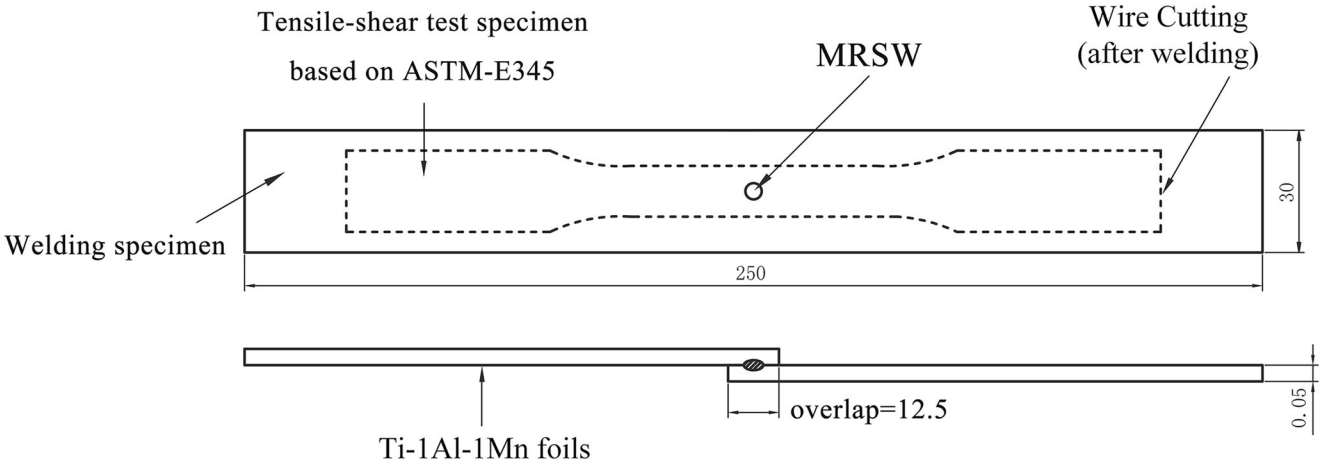


**Fig. 1** Welding and tensile-shear test specimens

The hybrid optimization method is displayed in Fig. 2 and is described in detail below.

Step1: Designing the experiments. Four important control factors were varied, namely, ramp time ($T_r$), welding time ($T_w$), welding current ($I$), and electrode force ($F$). The L27 Taguchi orthogonal array was chosen for the experimental design, as presented in Table 4.

Step2: Normalizing experimental responses. The experimental data were firstly normalized in the range 0–

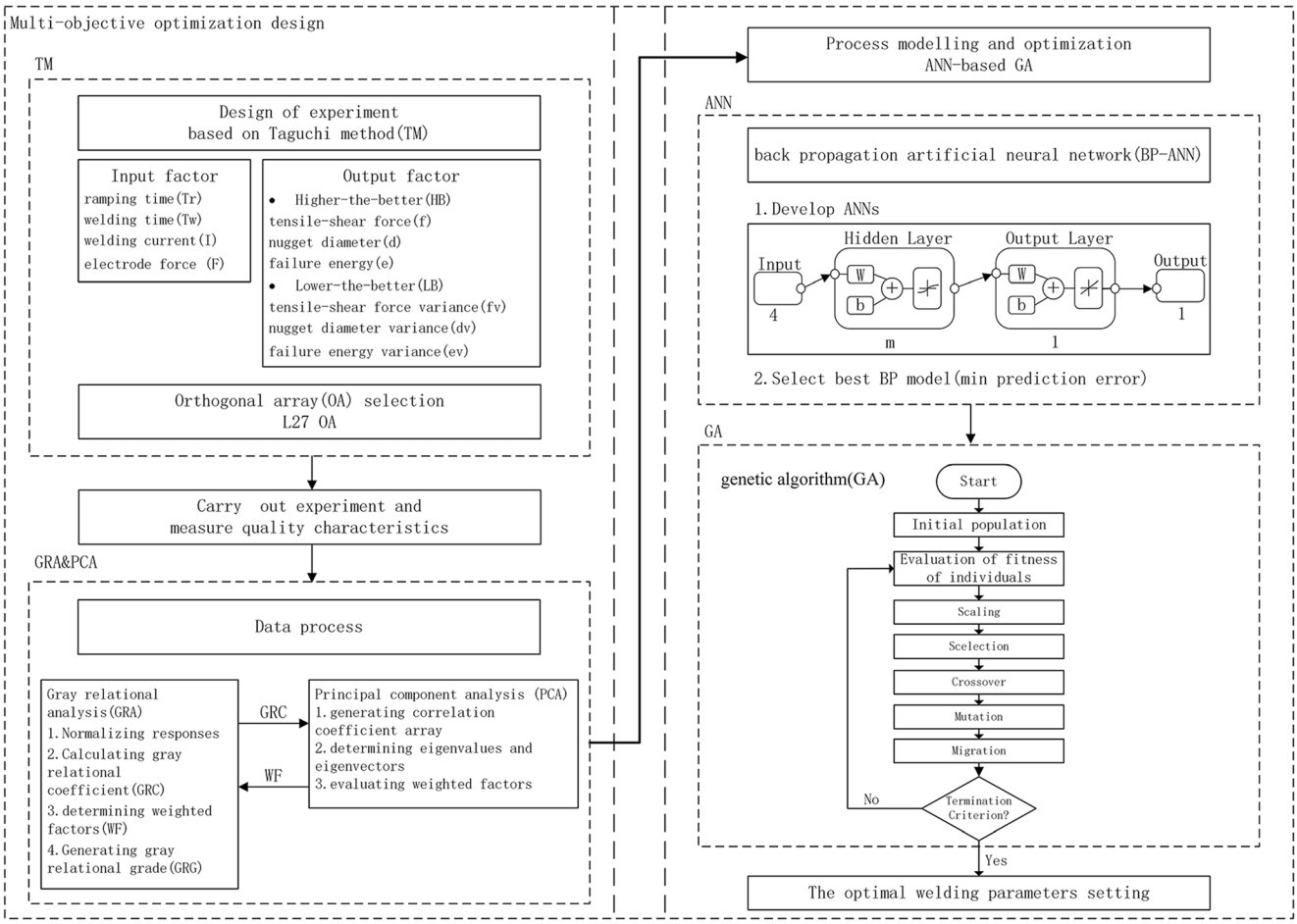


**Fig. 2** Steps of hybrid optimization approach

**Table 4** Taguchi $L_{27}$ orthogonal array design

| Serial no. | $T_1$ (ms) | $T_2$ (ms) | $I$ (A) | $F$ (N) |
|---|---|---|---|---|
| 1 | 1 | 4 | 400 | 8.89 |
| 2 | 1 | 4 | 600 | 17.6 |
| 3 | 1 | 4 | 800 | 35.2 |
| 4 | 1 | 6 | 400 | 17.6 |
| 5 | 1 | 6 | 600 | 35.2 |
| 6 | 1 | 6 | 800 | 8.89 |
| 7 | 1 | 8 | 400 | 35.2 |
| 8 | 1 | 8 | 600 | 8.89 |
| 9 | 1 | 8 | 800 | 17.6 |
| 10 | 3 | 4 | 400 | 8.89 |
| 11 | 3 | 4 | 600 | 17.6 |
| 12 | 3 | 4 | 800 | 35.2 |
| 13 | 3 | 6 | 400 | 17.6 |
| 14 | 3 | 6 | 600 | 35.2 |
| 15 | 3 | 6 | 800 | 8.89 |
| 16 | 3 | 8 | 400 | 35.2 |
| 17 | 3 | 8 | 600 | 8.89 |
| 18 | 3 | 8 | 800 | 17.6 |
| 19 | 5 | 4 | 400 | 8.89 |
| 20 | 5 | 4 | 600 | 17.6 |
| 21 | 5 | 4 | 800 | 35.2 |
| 22 | 5 | 6 | 400 | 17.6 |
| 23 | 5 | 6 | 600 | 35.2 |
| 24 | 5 | 6 | 800 | 8.89 |
| 25 | 5 | 8 | 400 | 35.2 |
| 26 | 5 | 8 | 600 | 8.89 |
| 27 | 5 | 8 | 800 | 17.6 |

**Table 5** Experimental data

| Serial no. | f | d | e | fv | dv | ev |
|---|---|---|---|---|---|---|
| 1 | 29.86 | 231.10 | 3.61 | 3.656 | 12.110 | 0.304 |
| 2 | 51.48 | 385.68 | 7.71 | 1.017 | 3.725 | 0.107 |
| 3 | 59.03 | 454.67 | 9.08 | 2.243 | 12.109 | 0.466 |
| 4 | 26.52 | 201.72 | 3.34 | 1.425 | 11.437 | 0.315 |
| 5 | 48.55 | 367.26 | 7.15 | 2.588 | 10.712 | 0.720 |
| 6 | 63.47 | 472.02 | 11.65 | 4.500 | 18.286 | 1.819 |
| 7 | 27.69 | 213.04 | 2.92 | 2.962 | 17.778 | 0.355 |
| 8 | 52.66 | 393.80 | 7.29 | 1.548 | 17.723 | 0.777 |
| 9 | 63.97 | 475.87 | 10.78 | 2.269 | 14.169 | 0.933 |
| 10 | 28.61 | 224.47 | 3.98 | 1.303 | 5.935 | 0.112 |
| 11 | 52.66 | 388.57 | 7.62 | 0.621 | 4.543 | 0.405 |
| 12 | 61.31 | 479.23 | 10.73 | 1.988 | 9.427 | 0.361 |
| 13 | 27.84 | 207.65 | 3.51 | 0.847 | 4.292 | 0.211 |
| 14 | 53.00 | 401.34 | 7.66 | 0.700 | 5.359 | 0.683 |
| 15 | 64.99 | 481.65 | 11.26 | 4.022 | 18.077 | 1.351 |
| 16 | 32.22 | 219.06 | 3.19 | 1.447 | 9.498 | 0.246 |
| 17 | 55.72 | 406.00 | 8.25 | 1.134 | 8.134 | 0.606 |
| 18 | 64.24 | 488.20 | 11.65 | 1.374 | 12.321 | 0.732 |
| 19 | 26.50 | 215.37 | 3.78 | 2.173 | 8.776 | 0.304 |
| 20 | 48.02 | 360.44 | 6.86 | 0.824 | 9.953 | 0.421 |
| 21 | 60.67 | 453.55 | 9.78 | 1.897 | 7.211 | 0.306 |
| 22 | 25.69 | 197.89 | 3.13 | 1.441 | 7.804 | 0.269 |
| 23 | 51.76 | 393.01 | 6.42 | 1.410 | 6.312 | 1.100 |
| 24 | 61.98 | 471.15 | 11.68 | 3.872 | 17.290 | 1.134 |
| 25 | 25.40 | 205.19 | 2.61 | 1.723 | 10.249 | 0.611 |
| 26 | 52.69 | 394.20 | 7.98 | 1.137 | 9.703 | 0.924 |
| 27 | 59.72 | 461.94 | 12.70 | 1.335 | 7.704 | 0.580 |

*f* tensile-shear force, *d* weld nugget size, *e* failure energy, *fv* variation of tensile-shear force, *dv* variation of weld nugget size, *ev* variation of failure energy

1. The processing for HB responses, namely tensile-shear force, weld nugget size, and failure energy, was done using Eq. (5) and the processing for LB responses, namely variations of tensile-shear force, weld nugget size, and failure energy, was done using Eq. (6):

$$y_j(i) = \frac{x_j(i) - x_j(i)^-}{x_j(i)^+ - x_j(i)^-} \tag{5}$$

$$y_j(i) = \frac{x_j(i)^+ - x_j(i)}{x_j(i)^+ - x_j(i)^-} \tag{6}$$

where $j = 1, 2, .....; I = 1, 2, .....; y_j(i)$ is the normalized value of $x_j(i)$ for the kth response; and $x_j(i)+$, $x_j(i)-$ are the maximum and minimum values of $x_j(i)$, respectively. The results are presented in Tables 5 and 6.

Step3: Calculating the gray relational coefficient. The gray relational coefficient was calculated using Eq. (7), as presented in Table 7:

$$\xi_j(i) = \frac{\Delta_{min} + \zeta \cdot \Delta_{max}}{\Delta_{0j}(i) + \zeta \cdot \Delta_{max}} \tag{7}$$

where

$$\Delta_{0k}(i) = |y_0(i) - y_j(i)|$$
$$\Delta_{min} = min\left(min\Delta_{0j}(i)\right), \Delta_{max} = max\left(max\Delta_{0j}(i)\right).$$

Here, $\Delta 0j(i)$, $y_0(i)$, and $y_j(i)$ are the deviation sequence, reference sequence, and comparative sequence, respectively, and $\xi \in (0, 1)$ is the distinguishing coefficient, which is usually set to 0.5.

Step4: Evaluating weighted factors for each response. PCA was employed to obtain the weighted factors for each response. Firstly, the gray relational coefficient was arranged in a matrix form, and then, some components were selected to account for the variance of the original multi-responses. The procedure is described as follows.

**Table 6** Normalized data $y_j$(i)

| Serial no. | $X_1$ | $X_2$ | $X_3$ | $X_4$ | $X_5$ | $X_6$ |
|---|---|---|---|---|---|---|
| 1 | 0.1126 | 0.1144 | 0.0988 | 0.2176 | 0.4242 | 0.8846 |
| 2 | 0.6586 | 0.6469 | 0.5050 | 0.8978 | 1.0000 | 1.0000 |
| 3 | 0.8494 | 0.8845 | 0.6413 | 0.5816 | 0.4243 | 0.7902 |
| 4 | 0.0281 | 0.0132 | 0.0723 | 0.7926 | 0.4704 | 0.8785 |
| 5 | 0.5848 | 0.5834 | 0.4498 | 0.4928 | 0.5202 | 0.6417 |
| 6 | 0.9615 | 0.9442 | 0.8953 | 0.0000 | 0.0000 | 0.0000 |
| 7 | 0.0578 | 0.0522 | 0.0307 | 0.3964 | 0.0349 | 0.8553 |
| 8 | 0.6885 | 0.6748 | 0.4634 | 0.7610 | 0.0387 | 0.6089 |
| 9 | 0.9743 | 0.9575 | 0.8094 | 0.5751 | 0.2827 | 0.5174 |
| 10 | 0.0810 | 0.0916 | 0.1354 | 0.8241 | 0.8482 | 0.9970 |
| 11 | 0.6885 | 0.6568 | 0.4967 | 1.0000 | 0.9438 | 0.8259 |
| 12 | 0.9071 | 0.9691 | 0.8042 | 0.6476 | 0.6084 | 0.8515 |
| 13 | 0.0616 | 0.0336 | 0.0888 | 0.9416 | 0.9610 | 0.9393 |
| 14 | 0.6972 | 0.7008 | 0.5000 | 0.9796 | 0.8878 | 0.6634 |
| 15 | 1.0000 | 0.9774 | 0.8573 | 0.1230 | 0.0144 | 0.2733 |
| 16 | 0.1723 | 0.0729 | 0.0575 | 0.7869 | 0.6036 | 0.9185 |
| 17 | 0.7658 | 0.7168 | 0.5588 | 0.8677 | 0.6972 | 0.7085 |
| 18 | 0.9811 | 1.0000 | 0.8960 | 0.8058 | 0.4097 | 0.6346 |
| 19 | 0.0276 | 0.0602 | 0.1159 | 0.5999 | 0.6531 | 0.8846 |
| 20 | 0.5714 | 0.5599 | 0.4214 | 0.9475 | 0.5723 | 0.8168 |
| 21 | 0.8910 | 0.8806 | 0.7100 | 0.6708 | 0.7606 | 0.8839 |
| 22 | 0.0073 | 0.0000 | 0.0518 | 0.7884 | 0.7199 | 0.9056 |
| 23 | 0.6659 | 0.6721 | 0.3778 | 0.7965 | 0.8224 | 0.4199 |
| 24 | 0.9240 | 0.9412 | 0.8983 | 0.1618 | 0.0684 | 0.4003 |
| 25 | 0.0000 | 0.0252 | 0.0000 | 0.7159 | 0.5520 | 0.7056 |
| 26 | 0.6892 | 0.6762 | 0.5317 | 0.8669 | 0.5895 | 0.5226 |
| 27 | 0.8668 | 0.9095 | 1.0000 | 0.8159 | 0.7267 | 0.7240 |

The gray relational coefficient of each response was represented as

$$T = \begin{bmatrix} \xi_1(1) & \xi_2(1) & \cdots & \cdots & \xi_n(1) \\ \xi_1(2) & \xi_2(2) & \cdots & \cdots & \xi_n(2) \\ \vdots & \vdots & \vdots & \vdots & \vdots \\ \xi_1(m) & \cdots & \cdots & \cdots & \xi_n(m) \end{bmatrix} = \begin{bmatrix} z_1(1) & z_2(1) & \cdots & \cdots & z_n(1) \\ z_1(2) & z_2(2) & \cdots & \cdots & z_n(2) \\ \vdots & \vdots & \vdots & \vdots & \vdots \\ z_1(m) & \cdots & \cdots & \cdots & z_n(m) \end{bmatrix}$$

where $m$ is the number of trials and $n$ is the number of responses.

Evaluation of the correlation coefficient array. The correlation coefficient matrix was calculated using Eq. (8), as presented in Table 8:

$$C_{jl} = \frac{Cov\left(z_j(i), z_l(i)\right)}{\sigma_{z_j}(i) * \sigma_{z_l}(i)} \tag{8}$$

where $j = 1, 2, \cdots\cdots, n$; $1 = 1, 2, \cdots\cdots, n$; Cov($z_j$(i), $z_l$(i)) is the covariance of sequences and $\sigma_{zj}$(i) is the standard deviation of the sequence.

Determination of the eigenvalues and eigenvectors. The eigenvalues corresponding to the eigenvectors were determined from a correlation coefficient array, as given in Table 9.

Evaluation of the weighted factors. In this experiment, all the principal components that corresponded to eigenvalues greater than 1 were selected to represent the original responses. Thus, the determination coefficient Cs was used to evaluate the contribution of each principal component to the weighted factors. The calculation method used Eq. (9), and the comprehensive weighted factors are listed in Table 10:

$$W_j = \left(\sum_{s=1}^{t} C_s * a_{sj}^2\right) / \left(\sum_{s=1}^{t} C_s\right) \tag{9}$$

where $W_j$ is the weighted factor for the jth response; $C_s$ is the determination coefficient, $\left(C_s = \frac{\lambda_s}{n}\right)$, λs is the eigenvalue; $a_{sj}$ is the eigenvector corresponding to eigenvalue λs; $t$ is the number of the first few principal components selected for evaluating the weighted factors; and $n$ is the number of experimental responses.

Step5: Generating a gray relational grade. After the weighted factors of each response were determined, the gray relational grade was calculated using Eq. (10), as presented in Table 11:

$$\gamma(i) = \sum_{j=1}^{n} W_j \cdot \xi_j(i) \tag{10}$$

where $\xi j$(i) is the gray relational coefficient and $W_j$ is the weighting factor for the jth response. It was found that the maximum value (0.7849) of the gray relational grade appeared in Serial no. 27.

Step6: Establishing a prediction model using a BP-ANN. The MATLAB neural network toolbox was used to establish a prediction model between a comprehensive performance index γ(i) and the four welding parameters. The BP-ANN approach was selected because of its high nonlinear mapping, self-study and self-adaptive properties, fault tolerance, and generalization ability.

The experimental data were divided into three groups: namely 1–9, 10–18, and 19–27. From each group, seven sets of randomly selected data were used to train the network and the remaining two sets of data were used for testing. Thus, 21 sets of data were selected for training the BP-ANN, and six sets of data were selected for independent testing. The learning rate (0.01) and momentum factor (0.9) were set. The termination condition of network training was when either the mean square error reached 0.0001 or 100 iterations were completed.

**Table 7** Gray relational coefficient $\xi_j(i)$

| Serial no. | $X_1$ | $X_2$ | $X_3$ | $X_4$ | $X_5$ | $X_6$ |
|---|---|---|---|---|---|---|
| 1 | 0.360386 | 0.360856 | 0.356847 | 0.389897 | 0.464760 | 0.812501 |
| 2 | 0.594280 | 0.586073 | 0.502489 | 0.830324 | 1.000000 | 1.000000 |
| 3 | 0.768478 | 0.812338 | 0.582308 | 0.544439 | 0.464796 | 0.704440 |
| 4 | 0.339707 | 0.336291 | 0.350220 | 0.706812 | 0.485624 | 0.804449 |
| 5 | 0.546330 | 0.545497 | 0.476101 | 0.496413 | 0.510294 | 0.582538 |
| 6 | 0.928539 | 0.899676 | 0.826871 | 0.333333 | 0.333333 | 0.333333 |
| 7 | 0.346689 | 0.345351 | 0.340301 | 0.453068 | 0.341276 | 0.775537 |
| 8 | 0.616172 | 0.605922 | 0.482358 | 0.676593 | 0.342150 | 0.561103 |
| 9 | 0.951146 | 0.921708 | 0.724055 | 0.540627 | 0.410753 | 0.508877 |
| 10 | 0.352367 | 0.355005 | 0.366409 | 0.739728 | 0.767143 | 0.994014 |
| 11 | 0.616108 | 0.592976 | 0.498354 | 1.000000 | 0.899027 | 0.741717 |
| 12 | 0.843349 | 0.941760 | 0.718557 | 0.586580 | 0.560815 | 0.770959 |
| 13 | 0.347602 | 0.340978 | 0.354318 | 0.895365 | 0.927726 | 0.891793 |
| 14 | 0.622829 | 0.625630 | 0.500000 | 0.960851 | 0.816718 | 0.597684 |
| 15 | 1.000000 | 0.956804 | 0.778006 | 0.363120 | 0.336558 | 0.407583 |
| 16 | 0.376590 | 0.350366 | 0.346612 | 0.701164 | 0.557757 | 0.859917 |
| 17 | 0.680968 | 0.638435 | 0.531228 | 0.790810 | 0.622848 | 0.631680 |
| 18 | 0.963649 | 1.000000 | 0.827775 | 0.720296 | 0.458569 | 0.577788 |
| 19 | 0.339591 | 0.347276 | 0.361250 | 0.555471 | 0.590390 | 0.812501 |
| 20 | 0.538453 | 0.531872 | 0.463564 | 0.905040 | 0.538965 | 0.731810 |
| 21 | 0.820963 | 0.807293 | 0.632943 | 0.603015 | 0.676220 | 0.811576 |
| 22 | 0.334955 | 0.333333 | 0.345268 | 0.702641 | 0.640927 | 0.841207 |
| 23 | 0.599440 | 0.603930 | 0.445556 | 0.710711 | 0.737871 | 0.462939 |
| 24 | 0.868004 | 0.894850 | 0.830955 | 0.373639 | 0.349262 | 0.454655 |
| 25 | 0.333333 | 0.339018 | 0.333333 | 0.637687 | 0.527411 | 0.629390 |
| 26 | 0.616684 | 0.606935 | 0.516371 | 0.789788 | 0.549140 | 0.511562 |
| 27 | 0.789631 | 0.846806 | 1.000000 | 0.730835 | 0.646592 | 0.644292 |

The optimum BP-ANN was selected as 4–11–1, because this gave the lowest prediction errors. The maximum error was less than 4%.

Step7: Determining the optimal welding parameters using the GA. After the BP-ANN was established, optimization of welding parameters for a higher comprehensive performance index was conducted using the GA. A fitness function was defined as the reciprocal of the comprehensive performance index calculated by the BP-ANN. The other GA parameters were as follows: a population size of 50 and a population type as a double vector; a stochastic uniform selection function; a crossover fraction of 0.8; a constant dependent mutation function; and a scattered crossover function.

**Table 8** Correlation matrix for each response

| | Z1 | Z2 | Z3 | Z4 | Z5 | Z6 |
|---|---|---|---|---|---|---|
| Z1 | 1.0000 | 0.9916 | 0.9117 | −0.2775 | −0.3070 | −0.6427 |
| Z2 | 0.9916 | 1.0000 | 0.9281 | −0.2769 | −0.3006 | −0.6103 |
| Z3 | 0.9117 | 0.9281 | 1.0000 | −0.2888 | −0.2927 | −0.5714 |
| Z4 | −0.2775 | −0.2769 | −0.2888 | 1.0000 | 0.7598 | 0.3824 |
| Z5 | −0.3070 | −0.3006 | −0.2927 | 0.7598 | 1.0000 | 0.5648 |
| Z6 | −0.6427 | −0.6103 | −0.5714 | 0.3824 | 0.5648 | 1.0000 |

Optimization was divided into two groups based on different search scopes. Group 1 was set to compare with the initial experiment, and group 2 was set to give full attention to the GA strength in global optimization. Thus, group 1 was set with lower limits of [1, 4, 400, 8.89] and upper limits of [5, 8, 800, 35.2]; group 2 was set with lower limits of [1, 4, 400, 5] and upper limits of [10, 10, 850, 50].

The optimal combination of welding parameters for mechanical quality and stability was found to be a ramp time of 2.484 ms, a welding time of 7.064 ms, a welding of 850 A, and an electrode force of 30.41 N. The comprehensive performance index was 0.9382 as predicted by BP-ANN in group 2, and $\gamma$ was 0.9083 in group 1 under the welding parameters of a ramp time of 2.668 ms, a welding time of 6.820 ms, a welding current of 800 A, and an electrode force of 31.620 N.

**Table 9** Eigenvalues, explained variation, and eigenvectors of each response

| Eigenvalues | Explained | Eigenvector | | | | | |
|---|---|---|---|---|---|---|---|
| 3.7875 | 0.6313 | − 0.4741 | − 0.4720 | − 0.4578 | 0.2823 | 0.3108 | 0.4082 |
| 1.4320 | 0.2387 | − 0.2882 | − 0.2970 | − 0.2814 | − 0.6055 | − 0.6087 | − 0.1114 |
| 0.4840 | 0.0807 | − 0.0954 | − 0.1600 | − 0.2344 | 0.4823 | − 0.0985 | − 0.8173 |
| 0.1890 | 0.0315 | − 0.0300 | − 0.0812 | − 0.0804 | − 0.5657 | 0.7231 | − 0.3784 |
| 0.1010 | 0.0168 | 0.4693 | 0.3570 | − 0.8022 | − 0.0323 | − 0.0092 | 0.0874 |
| 0.0065 | 0.0011 | 0.6797 | − 0.7276 | 0.0788 | 0.0052 | − 0.0168 | 0.0456 |

## 4 Results and discussion

### 4.1 Effects of welding parameters on responses

The interaction effects of the welding parameters on each response and the comprehensive performance index are shown in Fig. 3. Figure 3a–c shows that the parameters and their combinations have similar effects on the tensile-shear force, weld nugget size, and failure energy. When the welding current was increased from 400 to 800 A, the responses (f, d, e) all increased no matter how the other parameters ($T_r$, $T_w$, $F$) changed. This indicated that the interaction effects on the responses (f, d, e) between the welding current and the other parameters ($T_r$, $T_w$, $F$) were small. Furthermore, the interaction effects among the other parameters were also unnoticeable, except for that between welding time and electrode force. This is probably because, in contrast to NSRSW, the effect of welding current on these responses was far larger than the effects of the other parameters in MRSW. The changes of these responses, which were caused by variation in the other parameters, were thus hidden by the effect of the welding current. However, changing the welding time or electrode force would directly change the welding heat input, thereby changing the welding quality. When the welding current was constant, the interaction effect between the welding time and electrode force was evident.

As shown in Fig. 3b–g, the effects of the welding parameters on the responses (fv, dv, ev, $\gamma$) were different from the effects on the previous responses (f, d, e). The following differences could be determined:

1. The welding current still had an important influence on the responses (fv, dv, ev, and $\gamma$). However, the effects of other parameters also became evident.
2. At a welding current of 800 A, the tensile-shear force, nugget diameter, and failure energy achieved their highest values, and their variances were also at their highest levels. When the ramp time was 1 ms, the variances were large, but there was a value of the electrode force that brought the variances within a suitable range.
3. In addition to the interaction effect between welding time and electrode force, other interaction effects among welding parameters could also be observed.
4. The variation tendencies of the responses were no longer had a similarity with each other. Moreover, the variation tendency of $\gamma$ caused by the changes of welding parameters was different from those of all the other responses.

**Table 10** Weighted factors of each response

| | $W_1$ | $W_2$ | $W_3$ | $W_4$ | $W_5$ | $W_6$ |
|---|---|---|---|---|---|---|
| Value | 0.1859 | 0.1859 | 0.1738 | 0.1584 | 0.1717 | 0.1243 |

**Table 11** Gray relational grades

| Serial no. | $T_1$ (ms) | $T_2$ (ms) | $I$ (A) | $F$ (N) | Grade |
|---|---|---|---|---|---|
| 1 | 1 | 4 | 400 | 8.89 | 0.4387 |
| 2 | 1 | 4 | 600 | 17.6 | 0.7343 |
| 3 | 1 | 4 | 800 | 35.2 | 0.6487 |
| 4 | 1 | 6 | 400 | 17.6 | 0.4819 |
| 5 | 1 | 6 | 600 | 35.2 | 0.5244 |
| 6 | 1 | 6 | 800 | 8.89 | 0.6350 |
| 7 | 1 | 8 | 400 | 35.2 | 0.4146 |
| 8 | 1 | 8 | 600 | 8.89 | 0.5467 |
| 9 | 1 | 8 | 800 | 17.6 | 0.6934 |
| 10 | 3 | 4 | 400 | 8.89 | 0.5677 |
| 11 | 3 | 4 | 600 | 17.6 | 0.7164 |
| 12 | 3 | 4 | 800 | 35.2 | 0.7418 |
| 13 | 3 | 6 | 400 | 17.6 | 0.6016 |
| 14 | 3 | 6 | 600 | 35.2 | 0.6857 |
| 15 | 3 | 6 | 800 | 8.89 | 0.6649 |
| 16 | 3 | 8 | 400 | 35.2 | 0.5091 |
| 17 | 3 | 8 | 600 | 8.89 | 0.6484 |
| 18 | 3 | 8 | 800 | 17.6 | 0.7736 |
| 19 | 5 | 4 | 400 | 8.89 | 0.4809 |
| 20 | 5 | 4 | 600 | 17.6 | 0.6064 |
| 21 | 5 | 4 | 800 | 35.2 | 0.7252 |
| 22 | 5 | 6 | 400 | 17.6 | 0.5102 |
| 23 | 5 | 6 | 600 | 35.2 | 0.5980 |
| 24 | 5 | 6 | 800 | 8.89 | 0.6478 |
| 25 | 5 | 8 | 400 | 35.2 | 0.4528 |
| 26 | 5 | 8 | 600 | 8.89 | 0.6002 |
| 27 | 5 | 8 | 800 | 17.6 | 0.7849 |

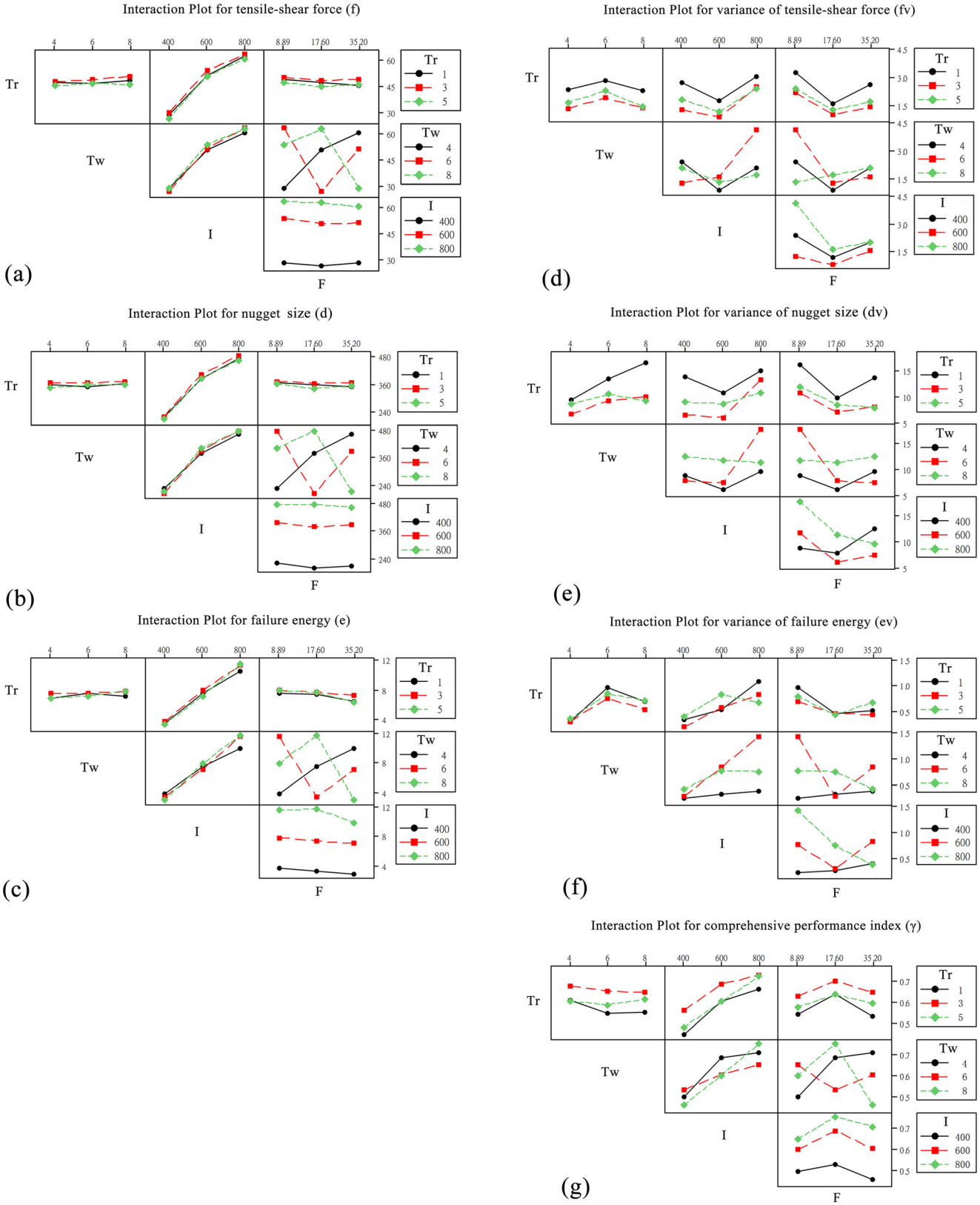


**Fig. 3** Interaction plot: **a** tensile-shear force; **b** variance of tensile-shear force; **c** nugget size; **d** variance of nugget size; **e** failure energy; **f** variance of failure energy; **g** comprehensive performance index

**Table 12** Confirmation experimental results corresponding to different welding parameters

| Performance | Welding conditions 1 | Welding conditions 2 | Welding conditions 3 |
|---|---|---|---|
| Tensile-shear force(N) | 59.72 | 60.92 | 63.21 |
| Nugget diameter(mm) | 461.94 | 468.46 | 483.19 |
| Failure energy($10^{-3}$ J) | 12.7 | 12.08 | 11.93 |
| Variance of tensile-shear force | 1.33 | 1.28 | 1.19 |
| Variance of nugget diameter | 7.70 | 5.62 | 6.79 |
| Variance of failure energy | 0.58 | 0.44 | 0.47 |
| Predicted value ($\gamma$) | 0.7895 | 0.9083 | 0.9382 |

The results of multi-objective and single-objective optimization were inevitably different. For excellent synthetic mechanical quality and stability, it is necessary to consider more than one response and to conduct multi-objective optimization.

### 4.2 Experimental validation

Validation experiments were conducted based on the optimization results. For convenience, the welding parameters were rounded to one decimal place. The welding parameters in group 1 were set as a ramp time of 2.7 ms, a welding time of 6.8 ms, a welding current of 800 A, and an electrode force of 31.6 N. The welding parameters in group 2 were set as a ramp time of 2.5 ms, a welding time of 7.1 ms, a welding current of 850 A, and an electrode force of 30.4 N. The experimental results are listed in Table 12; these correspond to the welding parameters recommended by original experimental design Serial no. 27, group 1 and group 2.

As discussed above, two sets of welding parameters were obtained using a hybrid optimization approach in different search scopes, namely welding conditions 2 and 3, as listed in Table 12. This was consistent with the experimental results, apart from a slight decrease in the failure energy; the joints that were welded under conditions 2 and 3 had greater tensile-shear carrying capacity, a larger nugget diameter, and a more-stable mechanical performance.

It also worth noting that the predicted $\gamma$ value under conditions 3 was greater than that under conditions 2; however, the synthetic performance displayed no significant increase between the two sets of experimental data. Apart from the values of the tensile-shear force and nugget size, the other responses even decreased slightly. This might have been caused by a lack of testing data at welding currents above 800 A, because the proposed model could not make the prediction well. The root cause of this was found to be that there was slight electrode sticking, when the welding current exceeded 800 A. Thus, the optimal welding parameters for maximum comprehensive performance index were set as a ramp time of 2.7 ms, a welding time of 6.8 ms, a welding current of 800 A, and an electrode force of 31.6 N, although some performances improved under conditions 3.

## 5 Conclusions

In this paper, multi-objective optimization design was conducted to find the best welding conditions for MRSW of ultra-thin Ti-1Al-1Mn foils. The following conclusions are drawn.

1. The responses could be converted into a comprehensive performance index for optimization based on the hybrid approach (GRA combined with PCA).
2. The set of optimal welding parameters for maximum comprehensive performance index was a ramp time of 2.7 ms, a welding time of 6.8 ms, a welding current of 800 A, and an electrode force of 31.6 N.
3. The welding current was the most important parameter for all the single responses and the comprehensive performance index. The interaction effect was not obvious among the welding parameters of tensile-shear force, weld nugget size, and failure energy. However, the interaction effects became significant in their variances.
4. The experimental results under optimal welding conditions of tensile-shear force, weld nugget size, failure energy, and their variances were found to be 60.92 N, 468.46 mm, $12.8 \times 10^{-3}$ J, 1.28, 5.62, and 0.44, respectively.

**Funding information** This work was supported by the Postgraduate Research & Practice Innovation Program of Jiangsu Province (grant no. KYCX17_0285). The authors were financially supported by the China Scholarship Council (grant no.201706830035).

## References


1. Cecil J, Kumar MBR, Lu Y, Basallali V (2016) A review of micro-devices assembly techniques and technology. Int J Adv Manuf Technol 83(9–12):1569–1581
2. Essa K, Modica F, Imbaby M, El-Sayed MA, ElShaer A, Jiang K, Hassanin H (2017) Manufacturing of metallic micro-components using hybrid soft lithography and micro-electrical discharge machining. Int J Adv Manuf Technol 91(1–4):445–452
3. Miao S-Y, Wang X-F, Yan C-L (2017) Self-roll-up Technology for Micro-Energy Storage Devices. Acta Phys -Chim Sin 33(1):18–27
4. Chang C-Y, Hu B-W (2018) Experimental study of hybrid extrusion rolling embossing process for replicating large-area micropattern devices. Int J Adv Manuf Technol 95(1–4):1003–1012
5. Yuhua C, Shuhan L, Dongya L, Wenming C (2017) Characteristics and mechanical properties of joints of Ti/Al dissimilar metal by micro resistance spot welding. Rare Metal Mater Eng 46:36–40
6. Wan X, Wang Y, Zhao D, Huang Y, Yin Z (2017) Weld quality monitoring research in small scale resistance spot welding by dynamic resistance and neural network. Measurement 99:120–127
7. Baskoro AS, Muzakki H, Kiswanto G (2018) Winarto effect of interlayer in dissimilar metal of stainless steel SS 301 and aluminum alloy AA 1100 using micro resistance spot welding. In: AIP Conference Proceedings, vol 1. AIP Publishing, p 040014
8. Mansor MSM, Yusof F, Ariga T, Miyashita Y (2018) Microstructure and mechanical properties of micro-resistance spot welding between stainless steel 316L and Ti-6Al-4V. Int J Adv Manuf Technol:1–15
9. Rao P Manufacturing Technology Foundry, Forming and Welding, 2008. Tata Mc Graw-Hill publishing company limited, New Delhi,
10. Jozwik P, Bojar Z, Kołodziejczak P (2010) Microjoining of Ni3Al based intermetallic thin foils. Mater Sci Technol 26(4):473–477
11. Park H, Kim T, Rhee S (2002) Optimization of welding parameters for resistance spot welding of TRIP steel using response surface methodology. Int J Kor Weld Soc 2(2):47–50
12. Kim T, Park H, Rhee* S (2005) Optimization of welding parameters for resistance spot welding of TRIP steel with response surface methodology. Int J Prod Res 43(21):4643–4657
13. Eşme U (2009) Application of TAGUCHI method for the optimization of resistance spot welding process. Arab J Sci Eng (Springer Science & Business Media BV) 34
14. Luo Y, Liu J, Xu H, Xiong C, Liu L (2009) Regression modeling and process analysis of resistance spot welding on galvanized steel sheet. Mater Des 30(7):2547–2555
15. Hamidinejad S, Kolahan F, Kokabi A (2012) The modeling and process analysis of resistance spot welding on galvanized steel sheets used in car body manufacturing. Mater Des 34:759–767
16. Wan X, Wang Y, Zhao D (2016) Multi-response optimization in small scale resistance spot welding of titanium alloy by principal component analysis and genetic algorithm. Int J Adv Manuf Technol 83(1–4):545–559
17. Zhao D, Wang Y, Liang D, Zhang P (2016) Modeling and process analysis of resistance spot welded DP600 joints based on regression analysis. Mater Des 110:676–684
18. Wan X, Wang Y, Zhao D (2016) Grey relational and neural network approach for multi-objective optimization in small scale resistance spot welding of titanium alloy. J Mech Sci Technol 30(6):2675–2682
19. Sun H, Yang J, Wang L (2017) Resistance spot welding quality identification with particle swarm optimization and a kernel extreme learning machine model. Int J Adv Manuf Technol 91(5–8): 1879–1887
20. Vignesh K, Perumal AE, Velmurugan P (2017) Optimization of resistance spot welding process parameters and microstructural examination for dissimilar welding of AISI 316L austenitic stainless steel and 2205 duplex stainless steel. Int J Adv Manuf Technol 93(1–4):455–465
21. Mirzaei F, Ghorbani H, Kolahan F (2017) Numerical modeling and optimization of joint strength in resistance spot welding of galvanized steel sheets. Int J Adv Manuf Technol 92(9–12):3489–3501
22. Boriwal L, Mahapatra M, Biswas P (2012) Modelling and optimizing the effects of process parameters on galvanized steel sheet resistance spot welds. Proc Inst Mech Eng B J Eng Manuf 226(4): 664–674
23. Thakur A, Nandedkar V (2014) Optimization of the resistance spot welding process of galvanized steel sheet using the Taguchi method. Arab J Sci Eng 39(2):1171–1176
24. Pashazadeh H, Gheisari Y, Hamedi M (2016) Statistical modeling and optimization of resistance spot welding process parameters using neural networks and multi-objective genetic algorithm. J Intell Manuf 27(3):549–559
25. Zhao D, Wang Y, Sheng S, Lin Z (2014) Multi-objective optimal design of small scale resistance spot welding process with principal component analysis and response surface methodology. J Intell Manuf 25(6):1335–1348
26. Zhao D, Wang Y, Wang X, Wang X, Chen F, Liang D (2014) Process analysis and optimization for failure energy of spot welded titanium alloy. Mater Des 60:479–489
27. Wan X, Wang Y, Zhao D (2016) Multiple quality characteristics prediction and parameter optimization in small-scale resistance spot welding. Arab J Sci Eng 41(5):2011–2021
28. El-Banna M, Filev D, Chinnam RB (2008) Online qualitative nugget classification by using a linear vector quantization neural network for resistance spot welding. Int J Adv Manuf Technol 36(3–4):237–248
29. Zhang H, Wang F, Xi T, Zhao J, Wang L, Gao W (2015) A novel quality evaluation method for resistance spot welding based on the electrode displacement signal and the Chernoff faces technique. Mech Syst Signal Process 62:431–443
30. Adams DW, Summerville CD, Voss BM, Jeswiet J, Doolan MC (2017) Correlating variations in the dynamic resistance signature to weld strength in resistance spot welding using principal component analysis. J Manuf Sci Eng 139(4):044502
31. Wan X, Wang Y, Zhao D, Huang Y (2017) A comparison of two types of neural network for weld quality prediction in small scale resistance spot welding. Mech Syst Signal Process 93:634–644
32. Wan X, Wang Y, Zhao D (2016) Quality monitoring based on dynamic resistance and principal component analysis in small scale resistance spot welding process. Int J Adv Manuf Technol 86(9–12):3443–3451
33. Chen S, Sun T, Jiang X, Qi J, Zeng R (2016) Online monitoring and evaluation of the weld quality of resistance spot welded titanium alloy. J Manuf Process 23:183–191
34. Xing B, Xiao Y, Qin QH, Cui H (2018) Quality assessment of resistance spot welding process based on dynamic resistance signal and random forest based. Int J Adv Manuf Technol 94(1–4):327–339
35. Chen F, Tong G, Yue X, Ma X, Gao X (2017) Multi-performance optimization of small-scale resistance spot welding process parameters for joining of Ti-1Al-1Mn thin foils using hybrid approach. Int J Adv Manuf Technol 89(9–12):3641–3650
36. Testing AASf, Materials (2009) Standard test methods for tension testing of metallic materials. ASTM international,
37. Gupta SK, Pandey KN, Kumar R (2018) Multi-objective optimization of friction stir welding process parameters for joining of dissimilar AA5083/AA6063 aluminum alloys using hybrid approach. P I Mech Eng L-J Mat 232(4):343–353
38. Porwal RK, Yadava V, Ramkumar J (2013) Modelling and optimisation of hole drilling electrical discharge micromachining process of Ti-6Al-4V thin sheet. Int J Precis Technol 3(2):183–205